

# Weak Adversarial Neural Pushforward Method for Fractional Fokker-Planck Equations

Andrew Qing He<sup>1</sup>      Wei Cai<sup>1</sup>

<sup>1</sup>Department of Mathematics, Southern Methodist University, Dallas, TX  
75275, USA

*Preprint — March 16, 2026*

## Abstract

We extend the Weak Adversarial Neural Pushforward Method (WANPM) to fractional Fokker-Planck equations (fFPE), in which the classical Laplacian diffusion operator is replaced by the fractional Laplacian  $(-\Delta)^{\alpha/2}$  for  $\alpha \in (0, 2]$ . The solution distribution is represented not as an explicit probability density function but as the pushforward of a simple base distribution through a time-parameterized neural network  $F_{\vartheta}(t, \mathbf{x}_0, \mathbf{r})$ , which enforces the initial condition exactly by construction. The weak formulation of the fFPE is discretized via Monte Carlo sampling entirely without temporal discretization, and the resulting min-max objective is optimized adversarially against a set of plane-wave test functions. A key computational advantage is that plane waves are eigenfunctions of the fractional Laplacian, so  $(-\Delta_x)^{\alpha/2} f = |\mathbf{w}|^{\alpha} f$  is computed exactly and at no additional cost for any  $\alpha$ . We validate the method on a one-dimensional fractional Fokker-Planck equation with a quadratic confining potential and  $\alpha = 1.5$ , using a particle simulation based on symmetric  $\alpha$ -stable Lévy increments as a benchmark. The learned solution faithfully reproduces the transient probability distribution over  $t \in [0, 2]$ , and robust statistics (median, IQR, MAD, and percentile bands) confirm close agreement with the particle simulation, while standard deviation comparisons highlight why second-moment metrics are inappropriate for heavy-tailed ( $\alpha < 2$ ) distributions. The present work lays the groundwork for mesh-free, scalable solvers for anomalous diffusion and fractional kinetics in high dimensions.

**Keywords:** fractional Fokker-Planck equation, fractional Laplacian, neural pushforward map, weak adversarial network, Lévy stable process, plane-wave test functions, anomalous diffusion.

**MSC (2020):** 65N75, 68T07, 35R11, 60G52.

## Contents

1 Introduction

2

<b>2</b>	<b>Fractional Fokker-Planck Equation and Its Weak Formulation</b>	<b>3</b>
2.1	Strong Form . . . . .	3
2.2	Weak Formulation . . . . .	4
2.3	Eigenfunction Property of Plane-Wave Test Functions . . . . .	5
<b>3</b>	<b>Weak Adversarial Neural Pushforward Method</b>	<b>5</b>
3.1	Pushforward Network Architecture . . . . .	5
3.2	Plane-Wave Test Functions . . . . .	5
3.3	Monte Carlo Discretization of the Weak Form . . . . .	6
3.4	Adversarial Min-Max Training . . . . .	7
<b>4</b>	<b>Particle Simulation as Ground Truth</b>	<b>7</b>
4.1	Symmetric $\alpha$ -Stable Lévy Increments . . . . .	7
<b>5</b>	<b>Numerical Results</b>	<b>8</b>
5.1	Problem Setup . . . . .	8
5.2	Training Configuration . . . . .	8
5.3	Training Convergence . . . . .	9
5.4	Transient Distribution Comparison . . . . .	9
5.5	Quantitative Comparison via Robust Statistics . . . . .	10
<b>6</b>	<b>Discussion and Outlook</b>	<b>11</b>
6.1	Strengths of the Approach . . . . .	11
6.2	Limitations and Caveats . . . . .	11
6.3	Relationship to the fBm Fokker-Planck Equation . . . . .	11
6.4	Future Directions . . . . .	11
<b>7</b>	<b>Conclusion</b>	<b>12</b>

# 1 Introduction

Fokker-Planck equations (FPEs) govern the evolution of probability density functions in stochastic dynamical systems and arise ubiquitously in statistical physics, chemistry, biology, and finance. Their classical form involves a second-order diffusion operator corresponding to Brownian noise; however, many natural phenomena exhibit anomalous diffusion driven by heavy-tailed Lévy processes rather than Gaussian noise. The appropriate PDE for such systems is the *fractional* Fokker-Planck equation (fFPE), in which the Laplacian diffusion term is replaced by the fractional Laplacian  $(-\Delta)^{\alpha/2}$  with  $\alpha \in (0, 2)$ . Fractional FPEs model superdiffusion in turbulent transport, charge carrier dynamics in amorphous semiconductors, and anomalous relaxation in complex fluids [1, 2].

Solving the fFPE in high dimensions poses formidable challenges. Classical finite-element or finite-difference discretizations of the fractional Laplacian require dense stiffness matrices whose assembly and storage become prohibitive even in modest dimensions. Spectral methods are effective in simple geometries but do not readily extend to curved or unbounded domains. Deep learning approaches, which have recently achieved remarkable success for classical high-dimensional PDEs, must contend with two additional obstacles in the fractional setting: (i) pointwise neural-network representations of the solution density require computing the fractional Laplacian of the network output, which involves

non-local integral operators and is expensive to evaluate; and (ii) the solution distribution may have heavy algebraic tails that a neural network density must resolve over an exponentially large effective domain.

In a companion paper [3] we introduced the Weak Adversarial Neural Pushforward Method (WANPM) for *classical* Fokker-Planck equations. The core idea is to represent the solution distribution as the pushforward of a tractable base distribution through a neural map  $F_{\mathcal{G}}$ , and to train  $F_{\mathcal{G}}$  adversarially against a family of plane-wave test functions so that the induced distribution satisfies the weak form of the FPE. This approach avoids explicit density evaluation, density normalization, and second-order backpropagation through the solution network.

The present paper extends WANPM to the fractional setting. The extension is both natural and computationally efficient: because plane waves are eigenfunctions of the fractional Laplacian, the action of  $(-\Delta)^{\alpha/2}$  on any test function  $f^{(k)}(t, x) = \sin(\mathbf{w}^{(k)} \cdot \mathbf{x} + \kappa^{(k)}t + b^{(k)})$  reduces to multiplication by  $|\mathbf{w}^{(k)}|^{\alpha}$ —an  $\mathcal{O}(1)$  operation per test function. This eigenfunction property means that changing from classical diffusion ( $\alpha = 2$ ) to fractional diffusion ( $\alpha < 2$ ) requires only a single parameter change in the loss computation; no quadrature of the non-local kernel is necessary.

Our contributions are as follows.

1. We derive the weak formulation of the time-dependent ffPE and show how it can be evaluated as Monte Carlo expectations with respect to the pushforward distribution, without discretizing time.
2. We describe the pushforward architecture and the fractional Laplacian eigenfunction property that makes plane-wave test functions exact and efficient for the fractional operator.
3. We implement and validate the method on a one-dimensional quadratic confining potential with  $\alpha = 1.5$ , comparing the learned transient distribution against a particle simulation using symmetric  $\alpha$ -stable Lévy increments.
4. We demonstrate that robust statistics—median, interquartile range (IQR), median absolute deviation (MAD), and percentile bands—are the appropriate comparison metrics for heavy-tailed distributions, and that standard deviation is unreliable for  $\alpha < 2$ .

The remainder of the paper is organized as follows. Section 2 presents the fractional Fokker-Planck equation and its weak formulation. Section 3 describes the neural pushforward architecture and the adversarial training procedure. Section 4 presents the particle simulation used as a ground-truth benchmark. Section 5 reports the numerical experiments. Section 6 discusses limitations and future directions.

## 2 Fractional Fokker-Planck Equation and Its Weak Formulation

### 2.1 Strong Form

Let  $X_t$  be a stochastic process on  $\mathbb{R}$  satisfying the Itô SDE

$$dX_t = b(X_t) dt + dL_t^{(\alpha)}, \quad X_0 \sim \rho_0, \quad (1)$$

where  $b : \mathbb{R} \rightarrow \mathbb{R}$  is a drift coefficient and  $L_t^{(\alpha)}$  is a symmetric  $\alpha$ -stable Lévy process with characteristic exponent  $\mathbb{E}[e^{i\xi L_t}] = e^{-t|\xi|^\alpha}$ . For  $\alpha = 2$  this reduces to standard Brownian motion with diffusivity 1. The probability density  $\rho(x, t)$  of  $X_t$  satisfies the fractional Fokker-Planck equation

$$\frac{\partial \rho}{\partial t} + (-\Delta_x)^{\alpha/2} \rho + \frac{\partial}{\partial x} [b(x)\rho] = 0, \quad (x, t) \in \mathbb{R} \times (0, T], \quad (2)$$

with initial condition  $\rho(x, 0) = \rho_0(x)$ . Here  $(-\Delta_x)^{\alpha/2}$  is the Riesz fractional Laplacian, defined spectrally by

$$\widehat{(-\Delta)^{\alpha/2} u}(\xi) = |\xi|^\alpha \hat{u}(\xi),$$

where  $\hat{u}$  denotes the Fourier transform. Equation (2) conserves probability:  $\int_{\mathbb{R}} \rho(x, t) dx = 1$  for all  $t \geq 0$ .

For the numerical experiments of this paper we take

$$b(x) = -kx, \quad k = 1, \quad (3)$$

corresponding to the gradient drift of a quadratic (harmonic) confining potential  $V(x) = \frac{1}{2}kx^2$ . With standard Brownian motion ( $\alpha = 2$ ), the solution is a Gaussian whose mean and variance can be tracked analytically. For  $\alpha < 2$  no closed-form expression for the density is available in general, and the solution develops algebraically decaying tails characteristic of  $\alpha$ -stable distributions.

**Remark 1** (Comparison with the fractional diffusion normalization). *Different conventions for the prefactor of  $(-\Delta)^{\alpha/2}$  appear in the literature. Our convention sets the coefficient to unity, so that the characteristic function of the Lévy increment over a unit time interval is  $e^{-|\xi|^\alpha}$ . The fractional diffusion coefficient can be absorbed into the wavenumber normalization of the test functions without loss of generality.*

## 2.2 Weak Formulation

Let  $f(t, x)$  be a smooth test function that decays sufficiently rapidly as  $|x| \rightarrow \infty$ . Multiplying (2) by  $f$  and integrating over  $\mathbb{R} \times [0, T]$  by parts in both space and time yields

$$\mathbb{E}_{\rho(T, \cdot)}[f(T, \cdot)] - \mathbb{E}_{\rho_0}[f(0, \cdot)] - \int_0^T \mathbb{E}_{\rho(t, \cdot)} \left[ \frac{\partial f}{\partial t} + \mathcal{L}f \right] dt = 0, \quad (4)$$

where the operator  $\mathcal{L}$  acts on the test function by

$$\mathcal{L}f = -(-\Delta_x)^{\alpha/2} f + b(x) \frac{\partial f}{\partial x}. \quad (5)$$

The identity  $(-\Delta_x)^{\alpha/2} f = |\xi|^\alpha \hat{f}$  ensures that  $\mathcal{L}f$  is well-defined for any smooth  $f$ , and the integration-by-parts step is valid whenever  $\rho$  has sufficient integrability.

**Remark 2** (Structure of the weak form). *Equation (4) decomposes into three Monte Carlo-evaluable expectations: a terminal expectation at  $t = T$ , an initial-condition expectation at  $t = 0$  (which can be computed from samples of  $\rho_0$  independently of the learned network), and an interior expectation integrated uniformly over  $[0, T]$ . This structure is identical to that of the classical FPE [3] up to the replacement of  $-\partial^2/\partial x^2$  by  $(-\Delta_x)^{\alpha/2}$  in the operator  $\mathcal{L}$ .*

## 2.3 Eigenfunction Property of Plane-Wave Test Functions

The central computational observation motivating our choice of test functions is the following. A spatial plane wave  $\phi_{\mathbf{w}}(x) = \sin(\mathbf{w} \cdot x + \varphi)$  or  $\cos(\mathbf{w} \cdot x + \varphi)$  satisfies

$$(-\Delta_x)^{\alpha/2} \phi_{\mathbf{w}}(x) = |\mathbf{w}|^\alpha \phi_{\mathbf{w}}(x), \quad (6)$$

which follows immediately from the Fourier-space definition of the fractional Laplacian. This identity is exact for all  $\alpha \in (0, 2]$  and all wavenumbers  $\mathbf{w}$ . In particular, for  $\alpha = 2$ , it reduces to  $-\partial^2 \phi_{\mathbf{w}} / \partial x^2 = |\mathbf{w}|^2 \phi_{\mathbf{w}}$ , consistent with classical differentiation.

As a consequence, the fractional part of  $\mathcal{L}f^{(k)}$  costs nothing extra to evaluate compared with classical diffusion: it is simply a multiplication by the scalar  $|\mathbf{w}^{(k)}|^\alpha$ . This makes the fFPE loss computation as cheap as the classical FPE loss computation, regardless of  $\alpha$ .

## 3 Weak Adversarial Neural Pushforward Method

### 3.1 Pushforward Network Architecture

We represent the solution distribution at each time  $t$  not by an explicit density but by a neural pushforward map

$$F_{\mathfrak{g}} : [0, T] \times \mathbb{R}^n \times \mathbb{R}^d \rightarrow \mathbb{R}, \quad (7)$$

where  $n = 1$  in our experiments and  $d$  is the dimension of a latent base distribution. Given  $x_0 \sim \rho_0$  and  $\mathbf{r} \sim \mathcal{N}(0, I_d)$ , the pushforward sample at time  $t$  is  $x(t) = F_{\mathfrak{g}}(t, x_0, \mathbf{r})$ . The induced distribution of  $x(t)$  is the learned approximation to  $\rho(\cdot, t)$ .

To enforce the initial condition exactly and to match the short-time diffusive scaling of Lévy processes, we parametrize

$$F_{\mathfrak{g}}(t, x_0, \mathbf{r}) = x_0 + \sqrt{t} \tilde{F}_{\mathfrak{g}}(t, x_0, \mathbf{r}), \quad (8)$$

where  $\tilde{F}_{\mathfrak{g}} : \mathbb{R}^{1+n+d} \rightarrow \mathbb{R}^n$  is a fully connected feedforward network with three hidden layers of width 128 and Tanh activation functions. At  $t = 0$ , the map reduces to the identity on  $x_0$ , so  $F_{\mathfrak{g}}(0, x_0, \mathbf{r}) = x_0 \sim \rho_0$  for any values of the network parameters. The  $\sqrt{t}$  prefactor is appropriate for diffusion-driven processes: the typical displacement of a Lévy process over time  $t$  scales as  $t^{1/\alpha}$ , and for  $\alpha$  near 2 (and exactly for  $\alpha = 2$ ) this is well-approximated by  $\sqrt{t}$  at short times.

The base distribution dimension  $d = 5$  was used in our experiments, providing the network with more latent degrees of freedom than the output dimension, which empirically improves the network’s ability to represent heavy-tailed distributions.

**Remark 3** (Overparameterized base distributions). *Allowing the base dimension  $d$  to exceed the target dimension  $n$  precludes the use of invertible (normalizing flow) architectures, which require  $d = n$ . This is not a limitation but a feature: the extra latent dimensions provide additional representational capacity without requiring Jacobian-determinant computations.*

### 3.2 Plane-Wave Test Functions

We parametrize the test functions as full space-time plane waves,

$$f^{(k)}(t, x) = \sin(w^{(k)}x + \kappa^{(k)}t + b^{(k)}), \quad k = 1, \dots, K, \quad (9)$$

where  $w^{(k)} \in \mathbb{R}$ ,  $\kappa^{(k)} \in \mathbb{R}$ , and  $b^{(k)} \in \mathbb{R}$  are trainable parameters. The derivatives required by the weak form (4) and the operator (5) are all available in closed form:

$$\frac{\partial f^{(k)}}{\partial t}(t, x) = \kappa^{(k)} \cos(w^{(k)}x + \kappa^{(k)}t + b^{(k)}), \quad (10)$$

$$\frac{\partial f^{(k)}}{\partial x}(t, x) = w^{(k)} \cos(w^{(k)}x + \kappa^{(k)}t + b^{(k)}), \quad (11)$$

$$(-\Delta_x)^{\alpha/2} f^{(k)}(t, x) = |w^{(k)}|^\alpha f^{(k)}(t, x), \quad (12)$$

where (12) follows from the eigenfunction property (6). No automatic differentiation through the test function is required.

The operator evaluated on the test function is therefore

$$\mathcal{L}f^{(k)}(t, x) = -|w^{(k)}|^\alpha f^{(k)}(t, x) + b(x) w^{(k)} \cos(w^{(k)}x + \kappa^{(k)}t + b^{(k)}). \quad (13)$$

### 3.3 Monte Carlo Discretization of the Weak Form

The three terms in the weak residual (4) are each approximated by Monte Carlo estimates.

**Terminal term.** Sample  $M_T$  tuples  $(x_0, \mathbf{r})$  with  $x_0 \sim \rho_0$  and  $\mathbf{r} \sim \mathcal{N}(0, I_d)$ , and evaluate the pushforward at  $t = T$ :

$$\hat{E}_T^{(k)} = \frac{1}{M_T} \sum_{m=1}^{M_T} f^{(k)}\left(T, F_{\mathfrak{g}}(T, x_0^{(m)}, \mathbf{r}^{(m)})\right). \quad (14)$$

**Initial condition term.** Sample  $M_0$  particles  $\tilde{x}^{(i)} \sim \rho_0 = \mathcal{N}(\mu_0, \sigma_0^2)$  and evaluate the test function at  $t = 0$ :

$$\hat{E}_0^{(k)} = \frac{1}{M_0} \sum_{i=1}^{M_0} f^{(k)}(0, \tilde{x}^{(i)}). \quad (15)$$

Note that  $f^{(k)}(0, x) = \sin(w^{(k)}x + b^{(k)})$ , so this term is computed from the known initial distribution and does not involve the pushforward network.

**Interior term.** Sample  $M$  triples  $(t^{(m)}, x_0^{(m)}, \mathbf{r}^{(m)})$  with  $t^{(m)} \sim \mathcal{U}[\epsilon, T]$ ,  $x_0^{(m)} \sim \rho_0$ , and  $\mathbf{r}^{(m)} \sim \mathcal{N}(0, I_d)$ , and form the pushforward  $x^{(m)} = F_{\mathfrak{g}}(t^{(m)}, x_0^{(m)}, \mathbf{r}^{(m)})$ :

$$\hat{E}^{(k)} = \frac{T}{M} \sum_{m=1}^M \left[ \frac{\partial f^{(k)}}{\partial t} + \mathcal{L}f^{(k)} \right] (t^{(m)}, x^{(m)}). \quad (16)$$

The factor  $T$  accounts for the uniform measure over  $[0, T]$ .

**Residual and loss.** For each test function  $k$ , the weak-form residual is

$$R^{(k)} = \hat{E}_T^{(k)} - \hat{E}_0^{(k)} - \hat{E}^{(k)}, \quad (17)$$

and the total training loss is

$$\mathcal{L}(\mathfrak{g}, \{\boldsymbol{\eta}^{(k)}\}) = \frac{1}{K} \sum_{k=1}^K (R^{(k)})^2, \quad (18)$$

where  $\boldsymbol{\eta}^{(k)} = \{w^{(k)}, \kappa^{(k)}, b^{(k)}\}$  are the test function parameters.

### 3.4 Adversarial Min-Max Training

The pushforward network and the test functions are trained adversarially:

$$\min_{\boldsymbol{\vartheta}} \max_{\{\boldsymbol{\eta}^{(k)}\}} \mathcal{L}(\boldsymbol{\vartheta}, \{\boldsymbol{\eta}^{(k)}\}). \quad (19)$$

The generator (pushforward network) is updated by gradient descent to minimize the loss, while the adversary (test function parameters) is updated by gradient ascent to maximize it, thereby searching for the plane-wave modes that are hardest to satisfy. The adversarial update provides an adaptive basis that concentrates on the frequency regime where the current learned distribution violates the weak form most severely.

The full procedure is summarized in Algorithm 1.

---

#### Algorithm 1 Weak Adversarial Neural Pushforward for ffPE

---

- 1: **Input:**  $K, M, M_0, M_T, N_{\text{epochs}}, \alpha, T, \rho_0$
  - 2: **Initialize:** pushforward network  $F_{\boldsymbol{\vartheta}}$ ; test function parameters  $\{w^{(k)}, \kappa^{(k)}, b^{(k)}\}_{k=1}^K$
  - 3: Optimizers: Adam (lr =  $10^{-3}$ ) for  $\boldsymbol{\vartheta}$ ; Adam (lr =  $10^{-2}$ ) for  $\boldsymbol{\eta}$
  - 4: **for** epoch = 1,  $\dots$ ,  $N_{\text{epochs}}$  **do**
  - 5:     Sample  $(t^{(m)}, x_0^{(m)}, \mathbf{r}^{(m)})$ ,  $\tilde{x}^{(i)}$ ,  $(x_0^T, \mathbf{r}^T)$  from respective distributions
  - 6:     Compute  $\mathcal{L}$  via (18)
  - 7:      $\boldsymbol{\vartheta} \leftarrow \boldsymbol{\vartheta} - \nabla_{\boldsymbol{\vartheta}} \mathcal{L}$  ▷ minimize over generator
  - 8:     **if** epoch mod 10 = 0 **then**
  - 9:         **for**  $j = 1$  to 5 **do**
  - 10:             Recompute  $\mathcal{L}$
  - 11:              $\boldsymbol{\eta} \leftarrow \boldsymbol{\eta} + \nabla_{\boldsymbol{\eta}} \mathcal{L}$  ▷ maximize over test functions
  - 12:             **end for**
  - 13:     **end if**
  - 14: **end for**
- 

## 4 Particle Simulation as Ground Truth

For  $\alpha < 2$ , no closed-form analytical solution for the density  $\rho(x, t)$  of equation (2) is available in the presence of a non-trivial drift. We therefore benchmark the neural solution against a particle simulation of the SDE (1).

### 4.1 Symmetric $\alpha$ -Stable Lévy Increments

The characteristic function of a symmetric  $\alpha$ -stable distribution with unit scale is  $e^{-|\xi|^\alpha}$ . Over a time step  $\Delta t$ , the SDE increment  $\Delta L^{(\alpha)}$  has scale  $(\Delta t)^{1/\alpha}$ . We generate increments using the Chambers-Mallows-Stuck algorithm [4] with  $\beta = 0$  (symmetry) and scale  $(\Delta t)^{1/\alpha}$ , implemented via `scipy.stats.levy_stable.rvs`.

The Euler-Maruyama discretization of (1) reads

$$X_{n+1} = X_n + b(X_n)\Delta t + \Delta L_n^{(\alpha)}, \quad (20)$$

with time step  $\Delta t = 0.01$  and  $N_{\text{particles}} = 10,000$ .

**Remark 4** (Variance and heavy tails). *For  $\alpha < 2$ , symmetric  $\alpha$ -stable distributions have infinite variance. In finite-sample particle simulations, the empirical variance fluctuates wildly from run to run due to rare but large excursions. This makes the standard deviation an unreliable comparison metric for  $\alpha < 2$ , as is clearly visible in our results. We therefore rely on robust statistics—median, IQR, MAD, and percentile bands—for all quantitative comparisons.*

## 5 Numerical Results

### 5.1 Problem Setup

We solve (2) with the quadratic drift (3) ( $k = 1$ ) on  $[0, T]$  with  $T = 2.0$  and  $\alpha = 1.5$ . The initial condition is a Gaussian centered at  $x_0 = 1.0$  with standard deviation  $\sigma_0 = 0.3$ ,

$$\rho_0(x) = \mathcal{N}(x; 1.0, 0.09). \quad (21)$$

Figure 1 illustrates the confining potential  $V(x) = \frac{1}{2}x^2$  and the initial density  $\rho_0$ . The initial distribution is centered at  $x = 1.0$ , offset from the potential minimum at  $x = 0$ , so that the drift pushes the distribution toward the origin while the fractional diffusion spreads it with algebraically decaying tails.

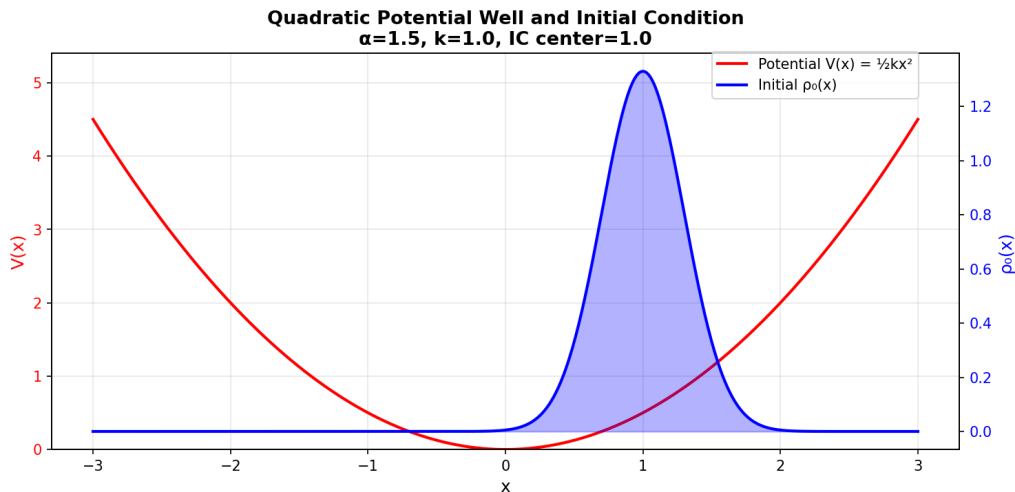


Figure 1: Quadratic confining potential  $V(x) = \frac{1}{2}kx^2$  (red, left axis) and initial condition  $\rho_0 = \mathcal{N}(1.0, 0.09)$  (blue, right axis) for the fractional Fokker-Planck experiment with  $\alpha = 1.5$ ,  $k = 1.0$ . The initial mass is offset from the potential minimum at  $x = 0$ ; the dynamics transport it toward the origin while fractional diffusion develops heavy tails.

### 5.2 Training Configuration

The pushforward network follows the architecture (8) with base dimension  $d = 5$  and three hidden layers of width 128. The initial distribution samples  $x_0 \sim \mathcal{N}(1.0, 0.09)$  are fed as the anchor point, and the latent noise  $\mathbf{r} \sim \mathcal{N}(0, I_5)$  provides stochastic variability.

We use  $K = 2,000$  plane-wave test functions (9), with spatial frequencies  $w^{(k)}$  initialized from  $\mathcal{N}(0, I)$  and normalized to unit norm, temporal frequencies  $\kappa^{(k)}$  initialized from  $\mathcal{N}(0, I)$ , and phase offsets  $b^{(k)}$  from  $\mathcal{U}[0, 2\pi]$ . Batch sizes are  $M = 2,000$  (interior),

$M_0 = M_T = 1,000$  (boundary terms). The adversarial update runs 5 gradient ascent steps every 10 epochs.

Training runs for  $N_{\text{epochs}} = 1,000$  epochs with the Adam optimizer ( $\text{lr} = 10^{-3}$  for the generator,  $\text{lr} = 10^{-2}$  for the test functions) and cosine annealing for the generator learning rate. Gradient clipping with maximum norm 1.0 is applied to both sets of parameters.

### 5.3 Training Convergence

Figure 2 shows the training loss and weak-form residual norm on log-scale axes over 1,000 epochs. Both curves exhibit a sharp initial descent spanning more than two orders of magnitude within the first 50 epochs, followed by a stabilization phase in which the loss oscillates around approximately  $10^{-2}$ . The oscillatory behavior is characteristic of adversarial min-max training: the test functions periodically find harder frequency modes to probe, causing transient spikes in the loss that the generator then suppresses. The overall convergence is stable and monotonically decreasing on a moving average, confirming that the adversarial dynamics do not lead to mode collapse or divergence.

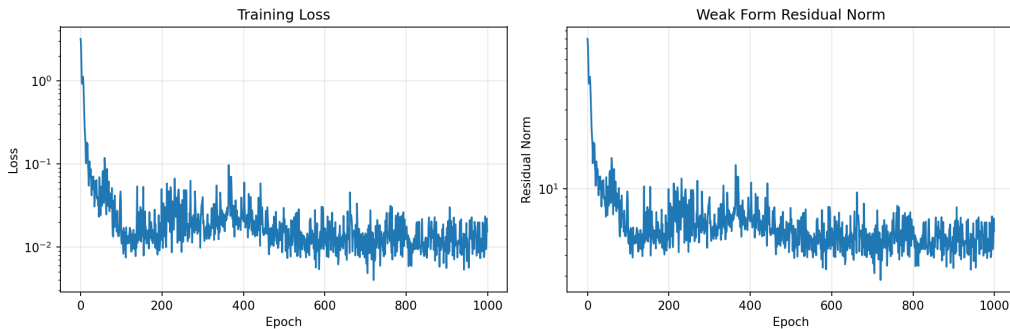


Figure 2: Training history over 1,000 epochs for the fractional Fokker-Planck problem with  $\alpha = 1.5$ . Left: training loss (18) on a log scale. Right:  $\ell^2$  norm of the weak-form residual vector  $(R^{(1)}, \dots, R^{(K)})$  on a log scale. Both curves exhibit the rapid initial convergence and adversarial oscillation typical of min-max training, with the loss stabilizing around  $10^{-2}$  and the residual norm around  $10^1$  (note that the residual norm is summed over  $K = 2,000$  test functions).

### 5.4 Transient Distribution Comparison

Figure 3 shows normalized histograms of the neural network samples (blue) alongside the particle simulation histogram (green) at eight evenly-spaced times  $t \in \{0.0, 0.2, 0.4, 0.6, 0.8, 1.0, 1.5, 2.0\}$ . At each time, 5,000 samples are drawn from the pushforward network and 10,000 particle simulation trajectories are used.

At  $t = 0$  both histograms accurately reproduce the initial Gaussian centered at  $x = 1.0$ . As time evolves, the distribution drifts toward the potential minimum at  $x = 0$  and develops the broad, algebraically decaying tails expected from  $\alpha$ -stable diffusion with  $\alpha = 1.5$ . The neural network distribution tracks this evolution faithfully throughout, capturing both the shift in the bulk of the distribution and the emergence of extended tails. By  $t = 1.5$  and  $t = 2$  the distribution has largely relaxed toward the fractional steady state, and the agreement between neural network and particle simulation remains good across the full support visible in the histograms.

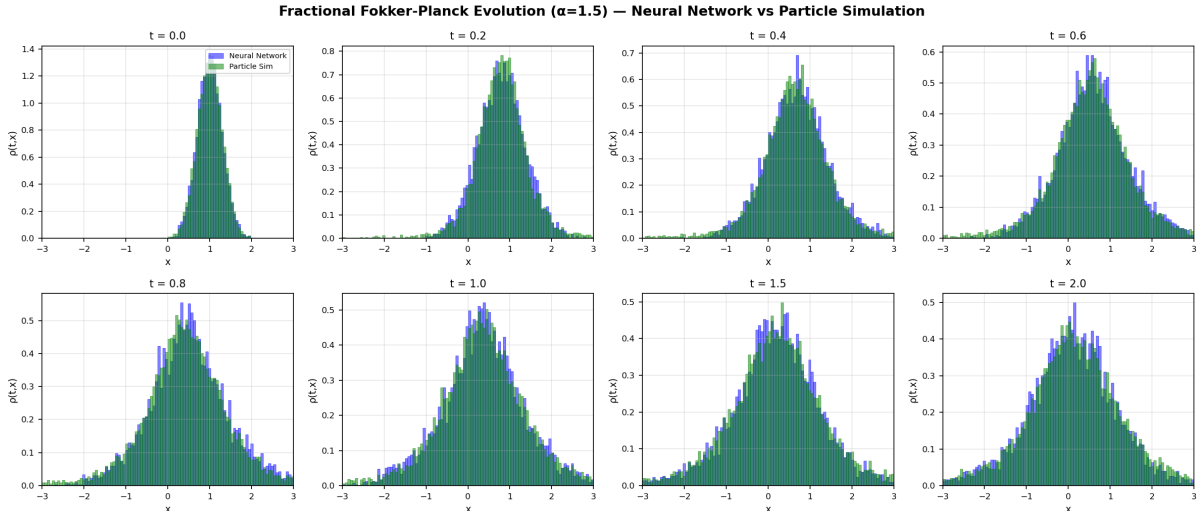


Figure 3: Fractional Fokker-Planck evolution ( $\alpha = 1.5$ ): neural network samples (blue) versus particle simulation (green) at eight time points. Both histograms are density-normalized over  $[-3, 3]$  with 100 bins. The neural network faithfully tracks the drift of the bulk toward the potential minimum at  $x = 0$  and the development of algebraically heavy tails over time.

## 5.5 Quantitative Comparison via Robust Statistics

Figure 4 reports six scalar metrics computed from 50 uniformly-spaced time snapshots over  $[0, 2]$ . Four robust metrics—mean, median, IQR, and MAD—show close tracking between neural network and particle simulation throughout the time interval. The median trajectories (upper right panel) are in particularly good agreement, with the neural network median following the particle simulation median through the entire relaxation process. The IQR and MAD curves (center row) both show the progressive widening of the distribution due to fractional diffusion, and the neural network correctly captures the rate of this spreading. The percentile band comparison (lower left) confirms that the 10th-to-90th-percentile spread is well-reproduced, with the neural network generating a distribution whose overall shape and extent match the particle simulation.

The lower right panel displays the standard deviation evolution and illustrates clearly why this metric is inappropriate for  $\alpha < 2$ . The particle simulation standard deviation exhibits large, erratic jumps due to occasional extreme sample values, while the neural network standard deviation is artificially stable because the pushforward map, being bounded during training, does not generate samples in the far tail with sufficient frequency to reproduce the divergent second moment. This contrast underscores the necessity of robust statistics for benchmarking heavy-tailed distributions.

The mean tracking (upper left panel) shows slightly noisier agreement than the median, as the mean is more sensitive to the tail behavior. Both mean curves nonetheless show the correct monotonic decrease from the initial center  $x = 1.0$  toward zero, with the discrepancy remaining within normal Monte Carlo sampling variability for  $K = 10,000$  particles.

Taken together, the robust metrics confirm that the learned pushforward distribution matches the particle simulation in location, scale, and spread throughout the time interval  $[0, 2]$ , validating the WANPM approach for fractional Fokker-Planck equations with  $\alpha = 1.5$ .

## 6 Discussion and Outlook

### 6.1 Strengths of the Approach

The extension of WANPM to fractional diffusion is notable for several reasons. First, the computational cost of evaluating the fractional Laplacian on plane-wave test functions is identical to the cost for classical diffusion: a single multiplication by  $|w^{(k)}|^\alpha$  per sample. This means the method scales to any  $\alpha \in (0, 2]$  without additional quadrature overhead. Second, the method remains purely mesh-free and requires no spatial discretization, making it in principle applicable to higher-dimensional fFPEs. Third, the pushforward representation naturally handles the heavy-tailed character of the solution by allowing the base distribution to be transformed into a distribution with extended support; the network does not need to represent the density itself, only its moments and cumulative statistics in the weak sense.

### 6.2 Limitations and Caveats

Several limitations should be acknowledged. The current experiments are one-dimensional, and scaling to higher dimensions requires further investigation of training stability, the number of test function modes  $K$  needed, and the interplay between the base distribution dimension  $d$  and the target dimension  $n$ . In the classical FPE companion paper [3] we have demonstrated scalability to 100 dimensions for standard diffusion; fractional diffusion in high dimensions remains to be explored.

The network’s capacity to resolve algebraic tails is inherently limited by the support of the pushforward samples seen during training. While the median and IQR match well, the far-tail behavior (beyond the 90th percentile) may not be reliably captured. This is a fundamental limitation of finite-sample Monte Carlo training and is not specific to our method.

Finally, for  $\alpha$  close to 0 the fractional Laplacian becomes nearly singular in frequency space, and the test-function weighting  $|w^{(k)}|^\alpha$  becomes nearly constant; the adversarial test function optimization may then struggle to identify informative modes. We have not explored this regime and leave it for future work.

### 6.3 Relationship to the fBm Fokker-Planck Equation

The implementation notes accompanying this paper also derive a weak formulation for the Fokker-Planck equation driven by fractional Brownian motion (fBm) with Hurst parameter  $H \in (0, 1)$ . In that setting the diffusion operator is non-local in *time* (due to the memory kernel of fBm) rather than non-local in *space*. The weak form contains a double integral over the triangular domain  $0 \leq s \leq t \leq T$ , which can be evaluated by a single 3D Monte Carlo without temporal discretization. This is a distinct generalization from the fractional Laplacian case studied here, and we leave its numerical validation to a forthcoming paper.

### 6.4 Future Directions

Immediate extensions include: (i) higher-dimensional fFPEs with gradient and non-gradient drifts; (ii) variable-order fractional operators  $\alpha(x)$ , which can model spatially inhomogeneous anomalous diffusion; (iii) tempered fractional Laplacians, which truncate

the heavy tails at a characteristic scale; and (iv) coupling with the fBm memory kernel for subdiffusive systems. On the methodological side, curriculum learning strategies for  $\alpha$  (analogous to the  $\sigma$ -annealing used in our triple-well experiments [3]) may improve training for small  $\alpha$ .

## 7 Conclusion

We have presented a weak adversarial neural pushforward method for the fractional Fokker-Planck equation with fractional Laplacian diffusion of order  $\alpha \in (0, 2]$ . The method combines three key ingredients: (i) a pushforward neural network that enforces the initial condition exactly via a  $\sqrt{t}$ -prefactored architecture; (ii) plane-wave test functions, which are exact eigenfunctions of the fractional Laplacian so that the operator cost is  $\mathcal{O}(1)$  for any  $\alpha$ ; and (iii) a fully Monte Carlo weak-form discretization without temporal mesh, enabling training from samples drawn directly from the product space  $[0, T] \times \rho_0 \times \pi_{\text{base}}$ .

Numerical validation on a one-dimensional quadratic confining potential with  $\alpha = 1.5$  demonstrates that the learned distribution accurately tracks the transient evolution over  $[0, 2]$ , as confirmed by robust statistical comparisons with a particle simulation using symmetric  $\alpha$ -stable Lévy increments. The results also confirm that standard deviation is an unreliable metric for heavy-tailed ( $\alpha < 2$ ) distributions and should be replaced by robust alternatives such as IQR and MAD.

The method is mesh-free, requires no density evaluation, no Jacobian computation, and no non-local quadrature, and its computational cost for the fractional operator is identical to that for classical diffusion. These properties make it a promising candidate for solving fractional Fokker-Planck equations in high dimensions.

## References

- [1] R. Metzler and J. Klafter, *The random walk's guide to anomalous diffusion: a fractional dynamics approach*, Physics Reports, **339**(1):1–77, 2000.
- [2] G. M. Zaslavsky, *Chaos, fractional kinetics, and anomalous transport*, Physics Reports, **371**(6):461–580, 2002.
- [3] A. Q. He and W. Cai, *Neural Pushforward Samplers for Transient Distributions from Fokker-Planck Equations with Weak Adversarial Training*, arXiv:2509.14575, 2025.
- [4] J. M. Chambers, C. L. Mallows, and B. W. Stuck, *A method for simulating stable random variables*, Journal of the American Statistical Association, **71**(354):340–344, 1976.
- [5] Y. Zang, G. Bao, X. Ye, and H. Zhou, *Weak adversarial networks for high-dimensional partial differential equations*, Journal of Computational Physics, **411**:109409, 2020.
- [6] M. Raissi, P. Perdikaris, and G. E. Karniadakis, *Physics-informed neural networks: A deep learning framework for solving forward and inverse problems involving nonlinear partial differential equations*, Journal of Computational Physics, **378**:686–707, 2019.

- [7] D. L. Scharfetter and H. K. Gummel, *Large-signal analysis of a silicon read diode oscillator*, IEEE Transactions on Electron Devices, **16**(1):64–77, 1969.
- [8] I. J. Goodfellow, J. Pouget-Abadie, M. Mirza, B. Xu, D. Warde-Farley, S. Ozair, A. Courville, and Y. Bengio, *Generative adversarial nets*, Advances in Neural Information Processing Systems, **27**, 2014.
- [9] L. Dinh, J. Sohl-Dickstein, and S. Bengio, *Density estimation using Real-valued Non-Volume Preserving (Real NVP) transformations*, arXiv:1605.08803, 2016.
- [10] J. Han, A. Jentzen, and W. E, *Solving high-dimensional partial differential equations using deep learning*, Proceedings of the National Academy of Sciences, **115**(34):8505–8510, 2018.
- [11] Y. Lipman, R. T. Q. Chen, H. Ben-Hamu, M. Nickel, and M. Le, *Flow matching for generative modeling*, International Conference on Learning Representations (ICLR), 2023.
- [12] N. M. Boffi and E. Vanden-Eijnden, *Probability flow solution of the Fokker-Planck equation*, Machine Learning: Science and Technology, **4**(3):035012, 2023.
- [13] Y. Song, J. Sohl-Dickstein, D. P. Kingma, A. Kumar, S. Ermon, and B. Poole, *Score-based generative modeling through stochastic differential equations*, International Conference on Learning Representations (ICLR), 2021.

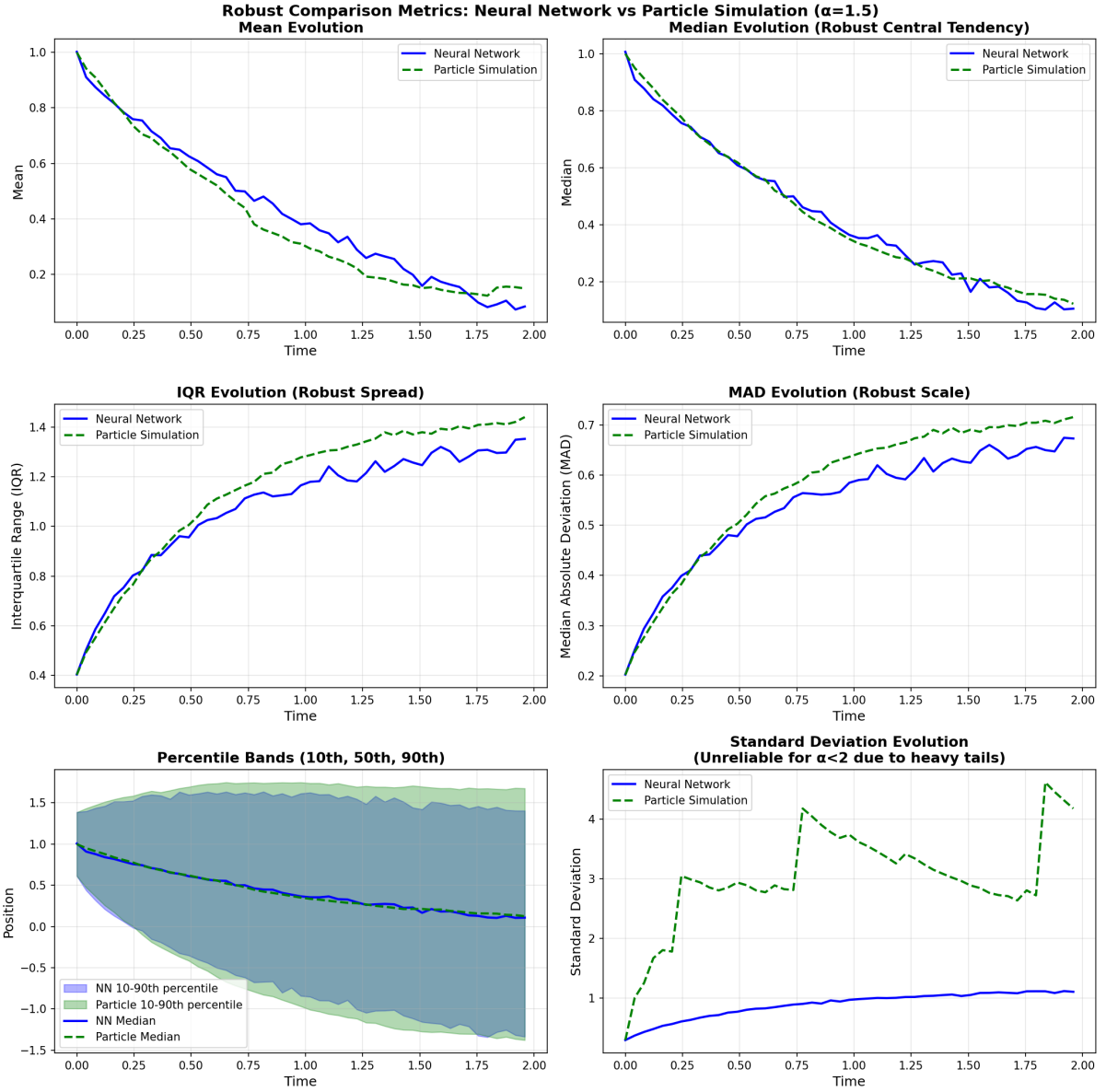


Figure 4: Robust comparison metrics over 50 time snapshots for the fractional Fokker-Planck problem ( $\alpha = 1.5$ ): mean (upper left), median (upper right), IQR (center left), MAD (center right), percentile bands (lower left), and standard deviation (lower right). The neural network (solid blue) closely tracks the particle simulation (dashed green) for all robust metrics. The standard deviation panel demonstrates the well-known instability of second-moment statistics for  $\alpha < 2$  Lévy processes: the particle simulation exhibits large jumps due to occasional extreme samples, while the neural network underestimates the tails. Standard deviation should not be used as a comparison metric for  $\alpha < 2$ .